Fall 2009

A Finite Element Approach to Model Electromagnetic Fields Scattered by a Buried Cavity

Nicole Pernischova

A FINITE ELEMENT APPROACH TO MODEL ELECTROMAGNETIC FIELDS SCATTERED BY A BURIED CAVITY

A Thesis

Submitted to McAnulty College

and Graduate School of Liberal Arts

Duquesne University

In partial fulfillment of the requirements for

the degree of Masters of Science

By

Nicole Pernischová

December 2009

A FINITE ELEMENT APPROACH TO MODEL ELECTROMAGNETIC FIELDS SCATTERED BY A BURIED CAVITY

By

Nicole Pernischová

Approved October 21, 2009

John Fleming, Ph.D. Assistant Professor of Mathematics (Dissertation Director)	Stacey Levine, Ph.D. Associate Professor of Mathematics (Committee Member)
Donald Simon, Ph.D. Associate Professor of Computer Science Director of Graduate Study (Committee Member)	Christopher M. Duncan, Ph.D. Dean McAnulty College and Graduate School of Liberal Arts

ABSTRACT

A FINITE ELEMENT APPROACH TO MODEL ELECTROMAGNETIC FIELDS SCATTERED BY A BURIED CAVITY

By

Nicole Pernischová

December 2008

Thesis supervised by Dr. John Fleming

This research investigates the plane-wave scattering from a two-dimensional arbitrarily shaped cavity embedded in an infinite metallic surface that has been covered with a layer or layers of dielectric material, considering both transverse electric and transverse magnetic polarizations. Due to the shape of the cavity, this problem is approached using the finite element method. This approach provides a boundary condition at the opening of the cavity which accounts for the effect of the overlayer(s) while confining the problem to the finite domain of the cavity itself. After determination of the solution for the electric and magnetic fields at the cavity aperture, the strength of the return echo can then be calculated and displayed in a radar cross section. In addition, numerical verifications and experiments illustrating the efficacy of the approach will be provided by comparison to other previously tested methods.

ACKNOWLEDGMENT

I would like to express my sincere gratitude to those who have offered assistance in the completion of my degree. It has been a pleasure working with most of Duquesne Mathematics and Computer Science faculty on this journey.

First, my advisor, Dr. John Fleming offered superior collaboration and guidance. I am also thankful for the encouragement and help of all the faculty members whether it was in the area of computer science, mathematics or statistics.

Last but not least, I would like to thank my boyfriend, Jeremy Gamret, and my family who always pushed me to reach for bigger goals, supported me and believed in me.

Contents

List of Figures

Chapter 1

Introduction

The study of electromagnetic plane scattering and radar cross section (RCS) measurements has been extensively investigated, specifically for the military aircraft development industry. There are many practical applications that require the knowledge of the RCS signature. An example is radar technology used to detect and locate aircraft, ships and missiles [32, 12].

A radar system emits electromagnetic waves towards a target, and by comparing the strength of the emitted wave to the return echo, displays the results in a RCS. The RCS of each object is unique and also dependent on the way in which the wave scatters from its surface. Thus it is important to analyze the effect that various surfaces have on the scattering profile [26]. Any inconsistency in a target's surface creates a different RCS signature, which has driven research to focus on the effect of gaps, cracks and seams on these profiles.

The accurate prediction and calculation of the RCS signature of targets is very important to the modern military because of different RCS enhancement applications [32, 12]. The military utilizes these types of predictions in camouflaging stealth aircraft, where the objective is to reduce the total RCS signature by minimizing the scattered energy from the surface of the body. Stealth aircraft proved their efficiency in the Persian Gulf War by utilizing the element of surprise in an attack while providing increased survival rates for American pilots.

There are also occasions where the military needs to enhance or alter the expected RCS

profile for defense purposes. For example, unmanned, remotely-piloted air vehicles are used to gather intelligence data or to saturate enemy air defense. This kind of vehicle is smaller in size than a fighter aircraft. Enhancing its RCS signature, however, reduces an enemy's capacity for distinguishing between it and a much larger fighter-size aircraft [12].

In either scenario, whether reducing the RCS or enhancing it, it is necessary to have efficient methods of calculating the RCS signatures of a scattering body. This can be accomplished by optimizing the design of the aircraft. The body shape and material coating can alter these signatures, and both factors should be considered when attempting to model accurate predictions.

The prediction of these scattering profiles has also been recognized as a possible nondestructive technique and is currently an important field of study for aircraft maintenance [5]. Typical maintenance procedures begin with stripping the aircraft surface of its coating in order to perform a visual inspection for signs of fatigue and cracks in the surface. Alternate methods for these inspections have been of interest due to costs associated with the process, and when considering the use of electromagnetic scattering, the ability to account for the material coating in predicting the RCS is essential. Parallel arguments can be made for the maintenance of other large metallic structures, such as bridges and buildings, where cost and time constraints are equally demanding.

1.1 Statement of the Problem

A small crack or seam in a metallic surface can be modeled by a channel in an infinite plane. (See Figure 2.1) This structure is visualized in three-dimensions, however the study of similar structures in two-dimensions offers computationally efficient approximations. Since the problem can be decomposed into two-dimensions, the interest is in seeking the results when the incident wave is of transverse electric (TE) and transverse magnetic (TM) polarization. Methods to determine the scattering in free space typically involve the use of Green's functions. The material layer over the surface and the material inside the cavity

adds much complexity to the problem of determining the field inside the cavity. An alternate approach is the use of the finite element method (FEM). In this project, a closed form solution of the plane wave inside the cavity space utilizes the FEM, then the restriction of this solution to the opening of the cavity determines the RCS of the scattered wave. The aim of this research is to investigate the two-dimensional scattering of an incident plane wave off the surface of a metal ground plane, with embedded arbitrary shaped cavity, that has been completely covered with a dielectric material.

1.2 Related Work

The importance of cavity problems in the computation of RCS started some extensive studies [1, 2, 3, 6, 14, 15, 16, 17, 18, 19, 31]. A two-dimensional cavity can be used to model long seams or cracks in metallic surfaces which can significantly contribute to the overall radar profile of large objects. There have been numerous techniques developed to account for the electromagnetic scattering from a cavity-backed aperture in a ground plane, including Fourier transform, finite element, integral equations, cavity mode coupling and impedance boundary conditions. These approaches are primarily applied to a problem with a material filled cavity in a perfect electrical conductor (PEC) ground plane that opens into an empty half space.

The Fourier transform technique was utilized by Park and Eom to examine the TE and TM scattering from a rectangular cavity embedded in an infinite ground plane [20, 23, 22]. The method computes a closed form solution by applying Fourier techniques and approximating a series solution for the field inside the cavity. The Fourier approach can be extended to the case of the cavity underneath an overlayer with appropriate modifications [7]. However, the Fourier solution is limited to the case of a rectangular cavity. When dealing with non-rectangular cavities, the Fourier approach is applicable in creating a boundary condition which can be incorporated to the FEM [28].

Integral equation methods are able to model arbitrarily shaped cavities embedded in

a ground plane. Analysis of the TM case of a material filled arbitrarily shaped cavity was analyzed by Wood using a set of scalar integral equations. Howes master's thesis expanded Wood's results to examine the results of the TE case [3, 12, 32, 31]. Integral equations can also be combined with the FEM to restrict the problem to a finite domain. The combined approach is known as the hybrid FE-BI (finite element integral equation) approach. Again, these techniques are not directly applicable to the case where the material layer or layers exist outside the cavity. To accommodate the overlayers the integral equation method could employ a Greens function for a layered media. The problem with the layered Greens function is that it is in the form of an infinite series [9]. Once an infinite series is included the important questions of convergence and truncation error are introduced into the problem. Therefore, an approach which does not need the Greens function will be more favorable.

An alternate solution to this problem was presented by Van and Wood which coupled the FEM with Fourier transforms, expressing the results of both the TM and TE case [28]. While this approach provides efficient solutions for an arbitrarily shaped cavity, the solution requires that the material is restricted to the cavity space below the half plane and that the upper half space is empty. Wood was able to account for this problem, and extended the research to consider the effect of over-filling the cavity space with a dielectric material. This was accomplished by creating an artificial boundary condition on a semi-circle containing the over-filled material region, and again combining a FEM with Fourier transforms to solve for the far field scattering [29, 30]. This methodology fails with the possibility of the entire surface being coated with a material layer due to the increasing size of the semi-circle needed to bound the material region.

When dealing with the problem of a cavity buried beneath a uniform layered material, the semicircular domain approach fails since no radius can contain the material outside of the cavity. The importance of such a problem is that a two-dimensional cavity beneath a layered material serves as a model of seams or cracks which are covered by paint or materials applied during a manufacturing process. These cracks and seems would be invisible

to a visual inspection but may be revealed by understanding the scattering characteristics of the cavity. The mathematical model can serve as a predictor of the scattering of electromagnetic waves by the buried cavity for use in non-destructive testing [5]. Therefore, it is important to be able to accommodate such a situation in cavity scattering computations.

The work proposed in this paper is an extension of previously published literature. A new boundary condition will be provided which restricts the problem to a finite domain yet properly accounts for the influence of the material layers. The FEM will be used to compute the fields in the finite cavity region. In order to apply the FEM, the boundary condition will be incorporated into the weak formulation of the problem.

1.3 Background

Electromagnetic waves are comprised of electric and magnetic components that oscillate transversely to one another, while also transversely to the direction of propagation. The relationship between these two components is best described mathematically by Maxwell's equations:

$$\nabla \times E = -\frac{\partial(\mu H)}{\partial t} \tag{1.1}$$

$$\nabla \times H = J + \frac{\partial(\varepsilon E)}{\partial t} \tag{1.2}$$

$$\nabla \cdot \varepsilon E = \rho_v \tag{1.3}$$

$$\nabla \cdot \mu H = 0 \tag{1.4}$$

where E and H are the electric and magnetic fields, respectively, J is the current density, ε is the permittivity of the medium, μ is the permeability of the medium and ρ_v is the free charge density.

In the problem described, the incident wave is the only source introduced into the problem, as free-space has no current or electric charge by definition, and a dielectric material is a non-conductive substance which also lacks a current and electric charge. Thus

$J = \rho = 0$. Applying this knowledge to the time-harmonic case where $E = \overline{E}e^{-\imath\omega t}$ is a shorter way of stating that $E(x, y, z, t) = \overline{E}(x, y, z)e^{-\imath\omega t}$, the time-varying forms are replaced by the corresponding phasor and $\frac{\partial}{\partial t}$ by $(-\imath\omega)$. Then Maxwell's equations are represented as:

$$\nabla \times \overline{E} = \imath\omega\mu\overline{H} \tag{1.5}$$

$$\nabla \times \overline{H} = -\imath\omega\varepsilon\overline{E} \tag{1.6}$$

$$\nabla \cdot \varepsilon\overline{E} = 0 \tag{1.7}$$

$$\nabla \cdot \mu\overline{H} = 0 \tag{1.8}$$

The wave equation for the electric field can be determined by eliminating the magnetic field from Maxwell's equations. Taking the curl of both side of equation 1.5 results in:

$$\nabla \times (\nabla \times \overline{E}) = \imath\omega\mu\nabla \times \overline{H}$$

Use equation 1.6 to substitute for $\nabla \times \overline{H}$, which results in the wave equation for the electric field as

$$\nabla \times \nabla \times \overline{E} = \omega^2\varepsilon\mu\overline{E}.$$

Using some vector calculus, $\nabla \times \nabla \times \overline{E}$ can be written as $-\triangle\overline{E} + \nabla(\nabla \cdot \overline{E})$.

Since $\nabla \cdot \overline{E} = 0$, the previous expression reduces to $-\triangle\overline{E}$, which can also be written as $-\nabla^2\overline{E}$.

Therefore the wave equation reduces to the so-called Helmholtz Equation

$$\triangle\overline{E} + k^2\overline{E} = 0 \tag{1.9}$$

where $k = \sqrt{\omega^2\mu\varepsilon}$ represents the wave number of the medium. Because $\overline{E}$ is a vector, the

Helmholtz Equation applies component-wise which means

$$\begin{aligned} \triangle E_x + k^2 E_x &= 0, \\ \triangle E_y + k^2 E_y &= 0, and \\ \triangle E_z + k^2 E_z &= 0. \end{aligned}$$

In a similar fashion, the wave equation for the magnetic field can be determined by eliminating the electric field, resulting in:

$$\triangle \overline{H} + k^2 \overline{H} = 0 \tag{1.10}$$

where $k = \sqrt{\omega^2 \mu \varepsilon}$ and it is also component-wise since $\overline{H}$ is a vector.

Maxwell's Equations give the foundation to the Helmholtz equation which are later used to determine important boundary and continuity conditions necessary for solving the back scatter and RCS from the buried cavity. The next chapter will describe the geometry, continuity and boundary conditions to find the solution if the wave lies inside the cavity. It also includes the RCS plots.

Chapter 2

Formulation of the Problem

2.1 Cavity Problem

In this paper, a solution is being sought given a two-dimensional model of the cavity problem. Thus without loss of generality, the entire geometry will be considered invariant in the z direction. Consider a two-dimensional infinite half plane comprised of an idealized metal, a PEC. An arbitrarily shaped cavity with the opening length L is embedded in the half plane. The entire conducting surface is covered with a thin dielectric material layer. (See Figure 2.1) The upper half above the PEC will consist of two regions. The upper most region, designated as region 0, contains a source-free medium that is time-invariant, homogeneous and linear, with electric permittivity ε_0 and magnetic permeability μ_0. It can be considered to be open space or air. Below is region 1, containing a dielectric material with electric permittivity ε_1 and magnetic permeability μ_1. Additionally, the cavity space below the half plane is defined as region 2 and contains a dielectric material with electric permittivity ε_2 and magnetic permeability μ_2. The thickness of the material layer atop of the ground plane is denoted as h; therefore the layer thickness ranges from $y = 0$ to $y = h$ [21].

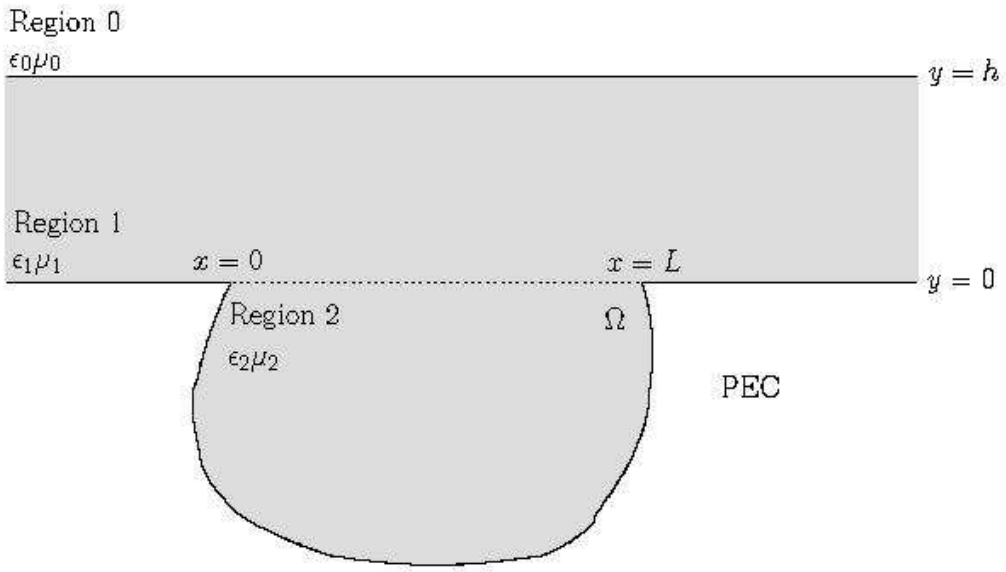

Figure 2.1: Material covered plane with a cavity

2.2 Boundary and Continuity Conditions

Boundary conditions are imposed at the interface between the two homogeneous regions, where the tangential electric component of a wave is always continuous on crossing a material boundary, and the tangential magnetic component of a wave is continuous across the boundary only if there does not exist a surface current on the boundary. Since it has been already established that a surface current does not exist between any of the three regions, the general boundary conditions can be considered:

$$\hat{n} \times (\overline{E}_0 - \overline{E}_1) = 0 \tag{2.1}$$

$$\hat{n} \times (\overline{E}_1 - \overline{E}_2) = 0 \tag{2.2}$$

$$\hat{n} \times (\overline{H}_0 - \overline{H}_1) = 0 \tag{2.3}$$

$$\hat{n} \times (\overline{H}_1 - \overline{H}_2) = 0 \tag{2.4}$$

where $\hat{n}$ is the normal vector to the surface.

Since the electric fields do not exist within the PEC, the boundary conditions outlined by equations 2.1 and 2.2 reduce to

$$\hat{n} \times \overline{E}_1 = 0 \tag{2.5}$$

$$\hat{n} \times \overline{E}_2 = 0 \tag{2.6}$$

at the planar surface and inside the cavity walls.

2.3 TM and TE

As previously stated, there are two polarizations and both are being considered in this research. The electromagnetic waves can be described on the xy-plane and are decomposed into these two polarizations:

1. If the electric component is perpendicular to the xy-plane, then the magnetic component is parallel to the xy-plane. Together, these two components form the TM field.

2. If the electric component is parallel to the xy-plane, then the magnetic component is perpendicular to the xy-plane. This situation creates the TE field.

Therefore, the two-dimensional scattering of a TM incident wave from an object's surface is measured independently of the scattering of a TE incident wave and the results of each polarization can be analyzed independently.

Since the parameters and the geometry are assumed to be invariant in the z-direction, the result is a two-dimensional problem. For TM polarization the fields have the form

$$\overline{E} = (0, 0, E_z) \qquad \overline{H} = (H_x, H_y, 0). \tag{2.7}$$

For TE polarization the fields have the form

$$\overline{E} = (E_x, E_y, 0) \qquad \overline{H} = (0, 0, H_z). \tag{2.8}$$

Throughout the paper, the notation u and v will be used to represent E_z and H_z respectively. When necessary, subscripts will be added to denote in which region the fields are contained. Also, the superscripts i and r will denote incoming and reflected or outgoing plane waves while s and t represent scattered and transmitted fields.

The scattering of the electromagnetic wave in the far field is a function of the plane wave at the cavity opening. Thus the first step in the proposed work is to determine the wave equation at this location. This solution requires careful consideration of the boundary conditions affecting the wave. A schematic detailing the incoming, reflected and scattered waves is provided in Figure 2.2. The total electric field of region 0, $\overline{E}_0$, is the summation of all electric fields of the area, where $\overline{E}_0 = u_0^i + u_0^r + u_0^s$. Likewise, the total electric field of region 1 and 2 are similarly determined by $\overline{E}_1 = u_1^i + u_1^r + u_1^s$ and $\overline{E}_2 = u_2^t$. Similar formulations for the total magnetic fields of each region can be derived.

The representation of an electromagnetic wave is dependent on the surrounding constraints and can take on various forms. The geometry in the described problem can be considered a combination of two entities, separated by the half plane. Below the half plane, the electromagnetic wave is bounded by the conducting walls. Above the half plane, the wave is only restricted by the continuity conditions across the material interface. These two representations can be coupled to solve for the finite element coefficients along the cavity opening and applied to the equation of the wave restricted by the cavity at the opening [21].

2.4 Approximation with Finite Element

If the shape of the cavity is rectangular, a Fourier Series can be used to find the solution, but this will not work for an arbitrarily shaped cavity. The FEM can produce an approximate solution for a cavity of any shape. The FEM originated in the field of structural analysis

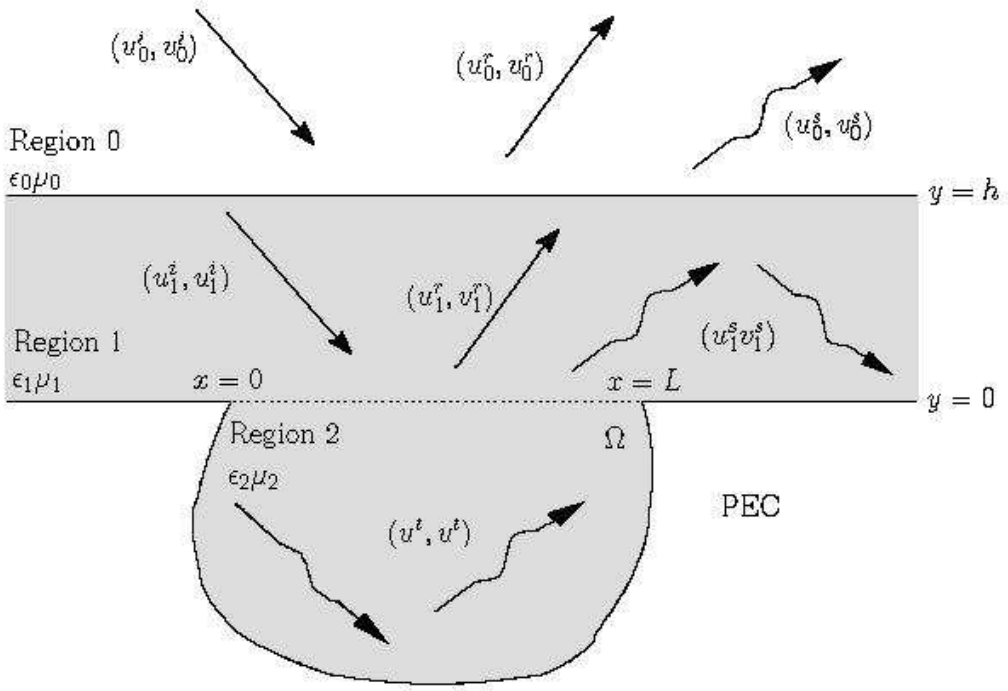

Figure 2.2: Field representations of the proposed geometry

and it was applied to electromagnetic problems in 1968. Even though the finite difference method and the method of moments are easier to program and conceptually simpler, FEM is more powerful for handling problems involving complex geometries and nonhomogeneous media.

The finite element analysis of any problem involves basically four steps [11]:

1. discretizing the solution region into a finite number of subregions or elements,
2. deriving governing equations for a typical element,
3. assembling of all elements in the solution region, and
4. solving the system of equations obtained.

In this setting, the discretization of the continuum involves dividing up the solution region, in this case region 2 or the cavity, into subdomains, called finite elements [25] (see figure 2.4). This triangular grid over the cavity consists of a set of piecewise linear basis

functions producing an approximation to the solution such that

$$u_2 \approx \sum_{i=1}^{N} \alpha_i \phi_i, \tag{2.9}$$

where the ϕ_i's are the known basis functions (see figure 2.4) and the α_i's are the unknown coefficients which will be computed.

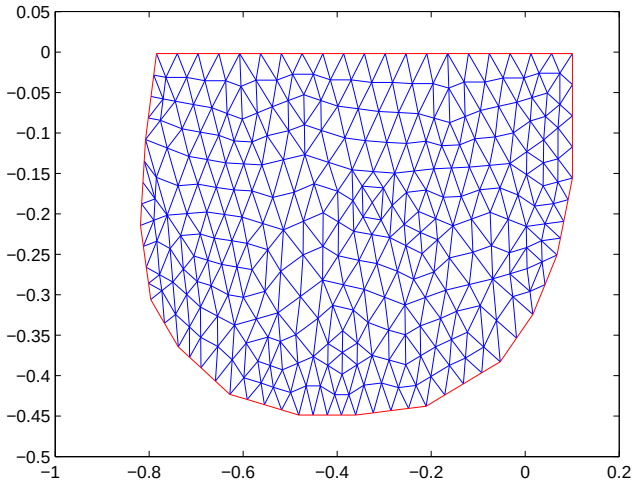

Figure 2.3: Triangular grid over the cavity

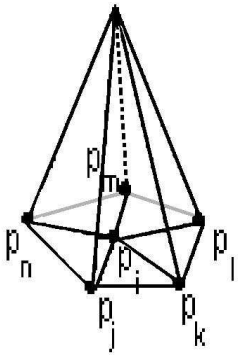

Figure 2.4: Basis function ϕ_i

2.5 Goals

The results of the magnetic and electric polarizations are analyzed separately in this paper, where the TM case is discussed first in Chapter Three, followed by the TE case in Chapter Four. Both of these chapters apply the necessary continuity and boundary conditions to solve for the coefficients of the finite element solution, which are then used to solve for the wave at the cavity opening. The RCS is then computed in Chapter Five based on the results from chapters three and four. The numerical results with differently shaped cavities and settings for both the TM and TE case, including RCS plots, are provided in Chapter Six. Lastly, Chapter Seven states the conclusion of this paper with suggested future research.

Chapter 3

TM Case

This chapter discusses the transverse magnetic part of the problem. Using equation 2.1, only the z component in the electric field plays a significant role. Therefore, $\overline{E} = (0, 0, u)$ where $u = E_z$. The Helmholtz Equation for this case can be written as

$$\triangle u + k^2 u = 0,$$

where $k^2 = \omega^2 \varepsilon \mu$. The notation u_j with $j = 0, 1, 2$ refers to the total fields in regions 0, 1 and 2 respectively. Solutions of Maxwell's equations satisfy two continuity conditions. These conditions state that the tangential component of the electric field $\overline{E}$ and the magnetic field $\overline{H}$ are continuous across material interfaces. From section 2.2 the electric continuity for TM case implies that

$$u_0 = u_1, \quad \text{at} \quad y = h \tag{3.1}$$

$$u_1 = u_2, \quad \text{at} \quad y = 0 \tag{3.2}$$

while the magnetic continuity implies that

$$\frac{1}{\mu_0}\frac{\partial u_0}{\partial y} = \frac{1}{\mu_1}\frac{\partial u_1}{\partial y}, \quad \text{at} \quad y = h \tag{3.3}$$

$$\frac{1}{\mu_1}\frac{\partial u_1}{\partial y} = \frac{1}{\mu_2}\frac{\partial u_2}{\partial y}, \quad \text{at} \quad y = 0. \tag{3.4}$$

Since the electric fields are zero inside a PEC material, $u = 0$ at $y = 0$ $[0, L]$ and at the walls of the cavity inside region 2.

In region 0, the total field consists of three parts. The known incoming plane wave is denoted as u_0^i. The plane wave reflected at the interface between regions 0 and 1 is denoted u_0^r. The scattered field is denoted as u_0^s. The total field u_0 is the sum of these three components $u_0 = u_0^i + u_0^r + u_0^s$ as mentioned in Chapter Two.

In region 1, u_1^i and u_1^r represent the plane waves due to the transmission of the incident field from region 0 and the reflection at the interface at the PEC material. The scattered field in region 1 is denoted u_1^s. The total field u_1 is the sum of these three components $u_1 = u_1^i + u_1^r + u_1^s$.

In region 2, the total field u_2 is the field transmitted into the cavity and it will not be decomposed into a superposition of fields. The FEM will be used to compute u_2 while enforcing the appropriate boundary conditions at the cavity walls as well as continuity conditions with the fields in region 1 above the cavity.

3.1 Incident and Reflected Fields

This section explains how to compute the fields u_0^r, u_1^i and u_1^r given the known incident plane wave u_0^i. These fields will be computed as if there was no cavity present and then considered as source fields which produce scattered and transmitted fields when interacting with the cavity region. They are computed only in region 0 and region 1 by enforcing the continuity of the electric and magnetic fields at $y = h$ and the PEC boundary condition at $y = 0$. When appropriate the notation $u_j^{ir} = u_j^i + u_j^r$ for $j = 0, 1$ will be used.

Since the material parameters are constant in both region 0 and region 1, a plane wave solution for the Helmholtz equation in both regions can be found. Solution for these incoming and outgoing plane waves is a result of applying the continuity conditions.

In region 0, the known incident plane wave is given as

$$u_0^i = e^{i\alpha_0 x + i\beta_0 y}. \tag{3.5}$$

Refer to figure 2.2 and consider it without the cavity. The total field in region 0 can be represented as the summation of incidence and reflected fields and the total field in region 1 as the summation of the incidence and reflected fields. To enforce continuity conditions, equation (3.1) at $y = h$ has to hold. Thus, the reflected field in region 0 can be written of the form

$$u_0^r = Ce^{i\alpha_0 x - i\beta_0 y}. \tag{3.6}$$

In region 1, there are incoming u_1^i and outgoing u_1^r plane waves

$$u_1^i = Ae^{i\alpha_1 x + i\beta_1 y} \tag{3.7}$$

$$u_1^r = Be^{i\alpha_1 x - i\beta_1 y}. \tag{3.8}$$

Using the basic theory of reflection and transmission of plane waves, $E_0 = E_1$ at $y = h$:

$$e^{i\alpha_0 x + i\beta_0 h} + Ce^{i\alpha_0 x - i\beta_0 h} = Ae^{i\alpha_1 x + i\beta_1 h} + Be^{i\alpha_1 x - i\beta_1 h} \tag{3.9}$$

$$e^{i\alpha_0 x}\left(e^{i\beta_0 h} + Ce^{-i\beta_0 h}\right) = e^{i\alpha_1 x}\left(Ae^{i\beta_1 h} + Be^{-i\beta_1 h}\right) \tag{3.10}$$

If $x = 0$

$$\left(e^{i\beta_0 h} + Ce^{-i\beta_0 h}\right) = \left(Ae^{i\beta_1 h} + Be^{-i\beta_1 h}\right) \tag{3.11}$$

$$e^{i\alpha_0 x} = e^{i\alpha_1 x}, \tag{3.12}$$

thus $\alpha_0 = \alpha_1$. The next steps follow from the continuity conditions:

$$\begin{aligned} k_0^2 &= \omega^2 \varepsilon_0 \mu_0 = \alpha_0^2 + \beta_0^2 \\ k_1^2 &= \omega^2 \varepsilon_1 \mu_1 = \alpha_1^2 + \beta_1^2 \\ &= \alpha_0^2 + \beta_1^2 \end{aligned}$$

$$\beta_1 = \sqrt{\omega^2 \varepsilon_1 \mu_1 - \alpha_1^2}.$$

In order to compute the coefficients A, B and C, enforce the continuity and boundary conditions. From the PEC boundary condition at $y = 0$,

$$Ae^{i\alpha_0 x} + Be^{i\alpha_0 x} = 0, \tag{3.13}$$

which reveals that $B = -A$. Therefore,

$$u_1^{ir} = Ae^{i\alpha_0 x + i\beta_1 y} - Ae^{i\alpha_1 x - i\beta_1 y} = Ae^{i\alpha_0 x}(e^{i\beta_1 y} - e^{-i\beta_1 y}). \tag{3.14}$$

Now, by enforcing the continuity of the electric field, $u_0^{ir} = u_1^{ir}$ at $y = h$ or

$$A(e^{i\beta_1 y} - e^{-i\beta_1 y}) - Ce^{-i\beta_0 h} = e^{i\beta_0 h}. \tag{3.15}$$

By enforcing the continuity of the magnetic field

$$\frac{1}{\mu_0}\frac{\partial u_0^{ir}}{\partial y} = \frac{1}{\mu_1}\frac{\partial u_1^{ir}}{\partial y}, \tag{3.16}$$

we obtain

$$A\frac{\mu_0}{\mu_1}\left(i\beta_1 e^{i\beta_1 h} + i\beta_1 e^{-i\beta_1 h}\right) + Ci\beta_0 e^{-i\beta_0 h} = i\beta_0 e^{i\beta 0h}. \tag{3.17}$$

Equations (3.15) and (3.17) provide a system of equations for the unknowns A and C. Use

Cramer's Rule to arrive at

$$A = \frac{2i\beta_0}{i\beta_0 e^{-i\beta_0 h}(e^{i\beta_1 h} - e^{-i\beta_1 h}) + \left(\frac{\mu_0}{\mu_1}\right) e^{-i\beta_0 h}(i\beta_1 e^{i\beta_1 h} + i\beta_1 e^{-i\beta_1 h})}$$

and

$$C = \frac{i\beta_0 e^{-i\beta_0 h}(e^{i\beta_1 h} - e^{-i\beta_1 h}) - \left(\frac{\mu_0}{\mu_1}\right) e^{i\beta_0 h}(i\beta_1 e^{i\beta_1 h} + i\beta_1 e^{-i\beta_1 h})}{i\beta_0 e^{-i\beta_0 h}(e^{i\beta_1 h} - e^{-i\beta_1 h}) + \left(\frac{\mu_0}{\mu_1}\right) e^{-i\beta_0 h}(i\beta_1 e^{i\beta_1 h} + i\beta_1 e^{-i\beta_1 h})}.$$

Once the coefficients of the incident and reflected field are obtained, the transmitted field u_2 inside the cavity can be computed. The interaction of the incident and reflected plane waves with cavity opening creates the transmitted field.

3.2 Artificial Boundary Condition

The goal of this section is to provide the representation of the scattered fields in regions 0 and 1 which are also created due to the interaction of the plane waves with the cavity. When there is the scattered field, the continuity conditions at the opening of the cavity are enforced. At this point, a boundary value problem is completely contained in region 2. The representations of the scattered fields are found using the Fourier theory and the fact that they must satisfy the Helmholtz equation. The representations in regions 0 and 1 are

$$u_0^s = \int_{-\infty}^{\infty} C(\lambda) e^{-\kappa_0 y} e^{2\pi i \lambda x} d\lambda \tag{3.18}$$

$$u_1^s = \int_{-\infty}^{\infty} [A(\lambda) e^{-\kappa_1 y} + B(\lambda) e^{\kappa_1 y}] e^{2\pi i \lambda x} d\lambda \tag{3.19}$$

where $\kappa_j = \sqrt{(2\pi\lambda)^2 - k_j^2}$ for $j = 0, 1$ and $A(\lambda)$, $B(\lambda)$, $C(\lambda)$ are the unknown Fourier transforms of the scattered field. The strategy will be to eliminate $A(\lambda)$ and $B(\lambda)$ from the

problem by employing the continuity conditions at $y = h$. Solve for $A(\lambda)$ and $B(\lambda)$ in terms of $C(\lambda)$ and substitute the solutions into equation (3.19). The electric field continuity gives $u_0^s = u_1^s$ and the magnetic continuity gives $\frac{1}{\mu_0}\frac{\partial u_0^s}{\partial y} = \frac{1}{\mu_1}\frac{\partial u_1^s}{\partial y}$ at $y = h$. These two conditions result in two equations:

$$C(\lambda)e^{-\kappa_0 h} = A(\lambda)e^{-\kappa_1 h} + B(\lambda)e^{\kappa_1 h} \tag{3.20}$$

$$-\kappa_0\left(\frac{\mu_1}{\mu_0}\right)C(\lambda)e^{-\kappa_0 h} = -\kappa_1 A(\lambda)e^{-\kappa_1 h} + \kappa_1 B(\lambda)e^{\kappa_1 h}. \tag{3.21}$$

Applying the above scattered field equations into the continuity conditions yields a system of equations that can be solved for A and B in terms of C using Cramer's Rule.

$$A(\lambda) = C(\lambda)\left[\frac{e^{(\kappa_1-\kappa_0)h}\left(\kappa_1 + \left(\frac{\mu_1}{\mu_0}\right)\kappa_0\right)}{2\kappa_1}\right] \tag{3.22}$$

$$B(\lambda) = C(\lambda)\left[\frac{e^{-(\kappa_0+\kappa_1)h}\left(\kappa_1 - \left(\frac{\mu_1}{\mu_0}\right)\kappa_0\right)}{2\kappa_1}\right] \tag{3.23}$$

Therefore, above $y = 0$ in region 1, the scattered field can be written in terms of a Fourier Transform. Substitute (3.22) and (3.23) into (3.19) to arrive at

$$u_1^s = \mathcal{F}_x^{-1}\left\{\left[\frac{R_{TM}(y)}{2\kappa_1}\right]C(\lambda)\right\}, \tag{3.24}$$

where $R_{TM}(y) = e^{(\kappa_1-\kappa_0)h}(\kappa_1 + \left(\frac{\mu_1}{\mu_0}\right)\kappa_0)e^{-\kappa_1 y} + e^{-(\kappa_0+\kappa_1)h}(\kappa_1 - \left(\frac{\mu_1}{\mu_0}\right)\kappa_0)e^{\kappa_1 y}$.
At $y = 0$,

$$\mathcal{F}_x[u_1^s] = \left[\frac{R_{TM}(0)}{2\kappa_1}\right]C(\lambda). \tag{3.25}$$

Use (3.25) to solve for $C(\lambda)$.

$$C(\lambda) = \left[\frac{2\kappa_1}{R_{TM}(0)}\right]\mathcal{F}_x[u_1^s] \tag{3.26}$$

The y-derivative of u_1^s from equation (3.24) has the following representation

$$\frac{\partial u_1^s}{\partial y} = \mathcal{F}_x^{-1}\left\{\left[\frac{S_{TM}(y)}{2}\right]C(\lambda)\right\},$$

where

$$S_{TM}(y) = -e^{(\kappa_1-\kappa_0)h}(\kappa_1 + \left(\frac{\mu_1}{\mu_0}\right)\kappa_0)e^{-\kappa_1 y} + e^{-(\kappa_0+\kappa_1)h}(\kappa_1 - \left(\frac{\mu_1}{\mu_0}\right)\kappa_0)e^{\kappa_1 y}.$$

When $y = 0$,

$$\frac{\partial u_1^s}{\partial y} = \mathcal{F}_x^{-1}\left\{\left[\frac{S_{TM}(0)}{2}\right]C(\lambda)\right\},$$

where

$$S_{TM}(0) = -e^{(\kappa_1-\kappa_0)h}(\kappa_1 + \left(\frac{\mu_1}{\mu_0}\right)\kappa_0) + e^{-(\kappa_0+\kappa_1)h}(\kappa_1 - \left(\frac{\mu_1}{\mu_0}\right)\kappa_0).$$

Substituting in (3.26) gives the following at $y = 0$

$$\frac{\partial u_1^s}{\partial y} = \mathcal{F}_x^{-1}\left[\Pi\mathcal{F}_x[u_1^s]\right] \tag{3.27}$$

where $\Pi = \frac{\kappa_1 S_{TM}(0)}{R_{TM}(0)}$.

The magnetic continuity condition at the cavity opening $(y = 0)$ yields

$$\frac{\partial u_2}{\partial y} = \frac{\mu_2}{\mu_1}\left(\frac{\partial u_1^s}{\partial y} + \frac{\partial u_1^{ir}}{\partial y}\right). \tag{3.28}$$

Enforcing the electric continuity conditions at $y = 0$, $u_2 = u_1^s + u_1^{ir}$. Since $u_1^{ir} = 0$ at $y = 0$, then $u_1^s = u_2$. Substitute u_2 into (3.27), then substitute (3.27) into (3.28) to arrive at

$$\frac{\partial u_2}{\partial y} = T(u_2) + g \tag{3.29}$$

where

$$T(u_2) = \left(\frac{\mu_2}{\mu_1}\right) \mathcal{F}_x^{-1}\left[\Pi \mathcal{F}_x[u_2]\right],$$

$$g = \left(\frac{\mu_2}{\mu_1}\right) \frac{\partial u^{ir}}{\partial y}.$$

Use (3.29) to restrict the problem to region 2 where a solution for u_2 will be found.

3.3 Finite Element Solution

Given the boundary condition from the previous section, the field (u_2) transmitted into the cavity will satisfy the following boundary value problem:

$$\triangle u_2 + k_2^2 u_2 = 0 \quad \text{in} \quad \Omega\text{(Region 2)}, \tag{3.30}$$

$$u_2 = 0 \quad \text{on} \quad \partial\Omega \backslash \{y = 0\}, \tag{3.31}$$

$$\frac{\partial u_2}{\partial y} = T(u_2) + g \quad \text{on} \quad \partial\Omega \cap \{y = 0\}. \tag{3.32}$$

Note that Ω represents the cavity (region 2).

As mentioned in section 2.4, the FEM can produce an approximate solution for the boundary value problem with a cavity of any shape. The Helmholtz Equation has a weak form used to find the solution. By multiplying both sides of the equation by one of the basis functions and integrating over the solution region Ω, we have

$$\int_\Omega \left[\frac{1}{\mu_2}\nabla^2 u_2 + k_0^2 \varepsilon_2 u_2\right] \phi_j d\Omega = 0. \tag{3.33}$$

Apply Green's identity to the first term of the integration. This weakens the derivatives to first order and creates the weak form of the Helmholtz equation:

$$\int_\Omega \nabla u_2 \cdot \nabla \phi_j d\Omega - \int_{\partial\Omega} \frac{\partial u_2}{\partial y} \phi_j d\Gamma + \int_\Omega k^2 u_2 \phi_j d\Omega = 0, \tag{3.34}$$

where ϕ_j is an appropriate test function. Note there is a boundary integral over $\partial\Omega$ and this term involves the normal derivative of the solution.

The boundary represents the opening of the cavity into the upper half space. Now assume there is a set of piecewise linear basis functions ϕ_i $i = 1, ..., N$ defined on the grid. The goal is to produce an approximate solution of the form $u_2 \approx \sum_{i=1}^{N} \alpha_i \phi_i$. This approximation is substituted into equation (3.34):

$$\int_{\Omega} \frac{1}{\mu_2} \nabla \left(\sum_{i=1}^{N} \alpha_i \phi_i \right) \cdot \nabla \phi_j d\Omega - \int_{\partial\Omega} \frac{\partial \left(\sum_{i=1}^{N} \alpha_i \phi_i \right)}{\partial y} \phi_j d\Gamma + \int_{\Omega} k_0^2 \varepsilon_2 \left(\sum_{i=1}^{N} \alpha_i \phi_i \right) \phi_j d\Omega = 0 \tag{3.35}$$

The basis functions ϕ_j are assumed to satisfy the PEC boundary condition at the cavity walls. Therefore, the boundary integral in the weak form can be written as

$$\int_{\partial\Omega} \frac{\partial \left(\sum_{i=1}^{N} \alpha_i \phi_i \right)}{\partial y} \phi_j d\Gamma = \int_{0}^{L} \frac{\partial \left(\sum_{i=1}^{N} \alpha_i \phi_i \right)}{\partial y} \phi_j dx. \tag{3.36}$$

Substituting in the transparent boundary condition gives

$$\int_{0}^{L} \frac{\partial \left(\sum_{i=1}^{N} \alpha_i \phi_i \right)}{\partial y} \phi_j dx = \int_{0}^{L} \left(T \left(\sum_{i=1}^{N} \alpha_i \phi_i \right) + g \right) \phi_j dx. \tag{3.37}$$

Therefore, for each basis function ϕ_j there is an equation

$$\begin{aligned} \int_{\Omega} \frac{1}{\mu_2} \nabla \left(\sum_{i=1}^{N} \alpha_i \phi_i \right) \cdot \nabla \phi_j d\Omega - \int_{0}^{L} T \left(\sum_{i=1}^{N} \alpha_i \phi_i \right) \phi_j dx \\ + \int_{\Omega} k_0^2 \varepsilon_2 \left(\sum_{i=1}^{N} \alpha_i \phi_i \right) \phi_j d\Omega = \int_{0}^{L} g \phi_j dx. \end{aligned} \tag{3.38}$$

These equations create a system which can be used to solve for the unknown coefficients α_j $j = 1, ..., N$.

Similar calculations will be discussed for the TE polarization in Chapter Four. Chapter Five shows the RCS computation for both polarizations.

Chapter 4

TE Case

This chapter discusses the transverse electric polarization of the problem. Again, consider the TE case, where the incoming and reflected fields are addressed first. Examination of the effect of the material layer with embedded cavity in the half plane takes place after determination of the incoming and reflected fields. These equations will then be used to determine a solution at the cavity opening.

In the TE case $\overline{H} = (0, 0, v)$, where $v = H_z$. Note that the TE case as well as the TM case has to satisfy all boundary and continuity conditions. As with the TM case, the field transmitted into the cavity (v_2) also satisfies the Helmholtz equation $\triangle v_2 + k^2 v_2 = 0$ where $k^2 = \omega^2 \varepsilon \mu$. Since v_2 represents the magnetic field, when PEC boundary condition is enforced, Maxwell's Equations show that $\frac{\partial v_2}{\partial n} = 0$ at the walls of the cavity.

4.1 Incident Field

The incoming and outgoing plane waves can be derived from equations in the TM case. Equation (3.5) is now $v_0^i = e^{i\alpha_0 x + i\beta_0 y}$, equation (3.6) is $v_0^r = De^{i\alpha_0 x - i\beta_0 y}$, equation (3.7) is $v_1^i = Ee^{i\alpha_0 x + i\beta_1 y}$ and equation (3.8) is $v_1^r = Fe^{i\alpha_0 x - i\beta_1 y}$ where $\beta_1 = \sqrt{\omega^2 \varepsilon_1 \mu - \alpha_0^2}$ and $\alpha_0 = \alpha_1$ using the same strategy as in the TM case. By enforcing the PEC boundary conditions at $y = 0$, $E = F$. Solve the system of equations for D and E by enforcing

continuity conditions at $y = h$:

$$D = \frac{2\left(\frac{\varepsilon_1}{\varepsilon_0}\right) i\beta_0}{\left(\frac{\varepsilon_1}{\varepsilon_0}\right) i\beta_0(e^{ih(\beta_1-\beta_0)} + e^{-ih(\beta_0+\beta_1)}) + i\beta_1(e^{ih(\beta_1-\beta_0)} - e^{-ih(\beta_0+\beta_1)})}$$

$$E = \frac{\left(\frac{\varepsilon_1}{\varepsilon_0}\right) i\beta_0(e^{ih(\beta_0+\beta_1)} + e^{ih(\beta_0-\beta_1)}) - i\beta_1(e^{ih(\beta_0+\beta_1)} - e^{ih(\beta_0-\beta_1)})}{\left(\frac{\varepsilon_1}{\varepsilon_0}\right) i\beta_0(e^{ih(\beta_1-\beta_0)} + e^{-ih(\beta_0+\beta_1)}) + i\beta_1(e^{ih(\beta_1-\beta_0)} - e^{-ih(\beta_0+\beta_1)})}.$$

Once the incoming and outgoing plane waves are computed in regions 0,1 they will then be used as source fields which produce scattered and transmitted fields when they interact with the cavity opening.

4.2 Artificial Boundary

Again, following the calculations in the TM case the scattered field in regions 0 and 1 can be represented as

$$v_0^s = \int_{-\infty}^{\infty} D(\lambda) e^{-\kappa_0 y} e^{2\pi i\lambda x} dx \tag{4.1}$$

$$v_1^s = \int_{-\infty}^{\infty} \left[E(\lambda) e^{-\kappa_1 y} e^{2\pi i\lambda x} + F(\lambda) e^{\kappa_1 y} e^{2\pi i\lambda x}\right] d\lambda \tag{4.2}$$

where $E(\lambda)$ and $F(\lambda)$ can be written in terms of $D(\lambda)$.

Enforcing the electric continuity at $y = h$ as in TM case equation (3.20), results in

$$D(\lambda)e^{-\kappa_0 h} = E(\lambda)e^{-\kappa_1 h} + F(\lambda)e^{\kappa_1 h}. \tag{4.3}$$

Enforcing the magnetic continuity at $y = h$, as in the TM equation (3.21), results in

$$-\kappa_0 \left(\frac{\varepsilon_1}{\varepsilon_0}\right) D(\lambda)e^{-\kappa_0 h} = -\kappa_1 E(\lambda)e^{-\kappa_1 h} + \kappa_1 F(\lambda)e^{\kappa_1 h}. \tag{4.4}$$

The equations (4.3) and (4.4) provide system of equations for which $E(\lambda)$ and $F(\lambda)$ can be solved in terms of $D(\lambda)$ using Cramer's Rule:

$$E(\lambda) = D(\lambda) \left[\frac{e^{(\kappa_1 - \kappa_0)h} \left(\left(\frac{\varepsilon_1}{\varepsilon_0} \right) \kappa_0 + \kappa_1 \right)}{2\kappa_1} \right] \tag{4.5}$$

$$F(\lambda) = D(\lambda) \left[\frac{e^{-(\kappa_1 + \kappa_0)h} \left(\left(\frac{\varepsilon_1}{\varepsilon_0} \right) \kappa_0 - \kappa_1 \right)}{-2\kappa_1} \right] \tag{4.6}$$

Substitute (4.5) and (4.6) into (4.2) to get

$$v_1^s = \mathcal{F}_x^{-1} \left\{ \left[\frac{R_{TE}(y)}{2\kappa_1} \right] D(\lambda) \right\} \tag{4.7}$$

where

$$R_{TE}(y) = e^{(\kappa_1 - \kappa_0)h} \left(\left(\frac{\varepsilon_1}{\varepsilon_0} \right) \kappa_0 + \kappa_1 \right) e^{-\kappa_1 y} - e^{-(\kappa_1 + \kappa_0)h} \left(\left(\frac{\varepsilon_1}{\varepsilon_0} \right) \kappa_0 - \kappa_1 \right) e^{\kappa_1 y}.$$

At $y = 0$,

$$\mathcal{F}_x[v_1^s] = \left[\frac{R_{TE}(0)}{2\kappa_1} \right] D(\lambda). \tag{4.8}$$

Take the $y-$derivative of v_1^s from equation (4.7) to arrive at

$$\frac{\partial v_1^s}{\partial y} = \mathcal{F}_x^{-1} \left\{ \left[\frac{S_{TE}(y)}{2} \right] D(\lambda) \right\} \tag{4.9}$$

where

$$S_{TE}(y) = -e^{(\kappa_1 - \kappa_0)h} \left(\left(\frac{\varepsilon_1}{\varepsilon_0} \right) \kappa_0 + \kappa_1 \right) e^{-\kappa_1 y} - e^{-(\kappa_1 + \kappa_0)h} \left(\left(\frac{\varepsilon_1}{\varepsilon_0} \right) \kappa_0 - \kappa_1 \right) e^{\kappa_1 y}.$$

Solve for $D(\lambda)$:

$$\frac{2}{S_{TE}(0)} \mathcal{F}_x \left[\frac{\partial v_1^s}{\partial y} \right] = D(\lambda). \tag{4.10}$$

When $y = 0$

$$\frac{\partial v_1^s}{\partial y} = \mathcal{F}_x^{-1}\left\{\left[\frac{S_{TE}(0)}{2}\right] D(\lambda)\right\} \tag{4.11}$$

where

$$S_{TE}(0) = -e^{(\kappa_1-\kappa_0)h}\left(\left(\frac{\varepsilon_1}{\varepsilon_0}\right)\kappa_0 + \kappa_1\right) - e^{-(\kappa_1+\kappa_0)h}\left(\left(\frac{\varepsilon_1}{\varepsilon_0}\right)\kappa_0 - \kappa_1\right).$$

Substituting in (4.10) at $y = 0$ gives

$$\frac{\partial v_1^s}{\partial y} = \mathcal{F}_x^{-1}\left[\frac{\kappa_1 S_{TE}(0)}{R_{TE}(0)}\mathcal{F}_x\left[v_1^s\right]\right]. \tag{4.12}$$

By enforcing the continuity conditions at the opening of the cavity ($y = 0$) $v_2 = v_1^s + v_1^{ir}$ and $\frac{\varepsilon_1}{\varepsilon_2}\frac{\partial v_2}{\partial y} = \frac{\partial v_1^s}{\partial y}$. Therefore at $y = 0$

$$v_2 = \mathcal{T}\left(\frac{\partial v_2}{\partial y}\right) + \mathcal{G} \tag{4.13}$$

where

$$\begin{aligned}
\mathcal{T}\left(\frac{\partial v_2}{\partial y}\right) &= \mathcal{F}_x^{-1}\left\{\Theta\mathcal{F}_x\left[\frac{\varepsilon_2}{\varepsilon_1}\frac{\partial v_2}{\partial y}\right]\right\} \\
\Theta &= \frac{\kappa_1 S_{TE}(0)}{R_{TE}(0)} \\
\mathcal{G} &= v_1^{ir}.
\end{aligned}$$

4.3 Finite Element Solution

Just like in the TM case, the FEM Solution uses a set of piecewise linear basis functions to produce an approximation to the solution such that $v_2 \approx \sum \alpha_i \phi_i$.

Consider the weak formulation

$$-\int_{\Omega} \nabla v_2 \cdot \nabla \phi_j d\Omega + \int_{\partial\Omega} \frac{\partial v_2}{\partial n} \phi_j d\Gamma + \int_{\Omega} k^2 v_2 \phi_j d\Omega = 0. \tag{4.14}$$

Note, there is a boundary integral over $\partial\Omega$ and this term represents the opening of the cavity into the layered material. Therefore it can be written as

$$\int_0^L \frac{\partial v_2}{\partial n} \phi_j dx.$$

In this case,

$$\frac{\partial v_2}{\partial y} \approx \sum_{i=1}^{M} \beta_i \psi_i.$$

Make a substitution for v_2 and $\frac{\partial v_2}{\partial y}$. Then multiply by the ψ_j function to get a system of equations that is used for computation of the solution.

$$\sum_{i=1}^{N} \alpha_i \phi_i = v_1^{ir} - \mathcal{T}\left(\frac{\partial v_2}{\partial y}\right) \tag{4.15}$$

For the interaction of ϕ and ψ functions, it is also needed to have

$$\int_a^b \left(\sum_{i=1}^{N} \alpha_i \phi_i\right) \psi_j dx = \int_a^b v_1^{ir} \psi_j dx - \sum_{i=1}^{M} \beta_i \int_{-\infty}^{\infty} \frac{\varepsilon_1}{\varepsilon_2} \Theta \mathcal{F}_x[\psi_i] \overline{\mathcal{F}_x[\psi_j]} dx. \tag{4.16}$$

Reproducing the equation (4.14) for each ϕ_j and reproducing the equation (4.15) for each ψ_j with the above results will provide a system which can be solved for the unknown α_i and β_i values. Once the α_i's and the β_i's are known, the finite element approximation of the solution of the transmitted field can be computed.

Chapter 5

Radar Cross Section Results

A radar system uses a transmitter to emit short pulses of electromagnetic waves towards a target and a receiver to record the strength of the return echo. A comparison of these two values are depicted in a RCS. The location of the receiver of this system can vary between the site emitting the source or multiple locations not at the source. When the transmitter and receiver are positioned at the same location, the incident and reflective angles of the plane waves are equal and the RCS is termed monostatic. In the case that a multisite radar system is used, the reflective angles differ from the incident angle and the RCS is termed bistatic. Chapter Six provides numerical results for both types of systems.

Once the cavity is illuminated by an incoming electromagnetic plane wave, the resulting effect is a scattering of the plane wave into the far field. Since we are interested in the intensity of the scattered energy, a technique must be employed to predict this quantity given the strength of the incoming wave and the cavity geometry. Since the cavity aperture lies within an infinite PEC, we can consider covering the opening with a conductor so that the image theory can be implemented. A surface can then be constructed on top of the infinite plane to produce equivalent electric (J) and magnetic (K) sources, where:

$$\overline{J_1} = \hat{n} \times \overline{H_1} \tag{5.1}$$

$$\overline{K_1} = \overline{E_1} \times \hat{n}. \tag{5.2}$$

Applying the method of images guarantees that the PEC plane can be removed and the combination of the original charge configuration that originally laid above the PEC and the image configuration is electrically equivalent to the original charge configuration in the presence of the PEC. This process eliminates the electric source, leaving a doubled magnetic source located along the cavity aperture. The far field components of the electric field are computed from the resulting sources, and from this the RCS is configured by taking the norm of the squared far field values [24].

The general form of the two-dimensional scattering cross section for the TM and TE polarization is

$$\sigma_{TM}(\phi, \phi^i) = \frac{k_0}{4} \left| \int \int \left(\eta J_z + K_x \sin\phi - K_y \cos\phi \right) e^{\imath k_0 (x' \cos(\phi + y' \sin(\phi)))} dx' dy' \right|^2 \tag{5.3}$$

$$\sigma_{TE}(\phi, \phi^i) = \frac{k_0}{4} \left| \int \int \left(J_x \sin\phi - J_y \cos\phi - \frac{K_z}{\eta} \right) e^{jk(x' \cos\phi + y' \sin\phi)} dx' dy' \right|^2, \tag{5.4}$$

where $\eta = \sqrt{\frac{\mu_0}{\varepsilon_0}}$, J_x, J_y and J_z represents the electric current of the x, y and z components, K_x, K_y and K_z represents the magnetic current of the x, y and z components. Additionally, the value of y' is fixed, such that if there does not exist a material layer above the cavity surface, $y' = 0$, otherwise, $y' = h$ [24].

The results of the image process revealed that our RCS is a function of only magnetic sources at the cavity aperture, thus eliminating J from our equations. Additionally, the magnetic sources as determined by equation (5.1) are a function of the electric field. In the TM polarization, the electric field is invariant in the z direction, where the product of this function with the normal results in the magnetic sources only existing in the x direction. Likewise, for the TE polarization, the electric field is invariant in the x direction, which

results in the magnetic sources existing in the z direction. Applying these facts reduces the equations representing the RCS to

$$\sigma_{TM}(\phi,\phi^i) = \frac{k_0}{4}\left|\int K_x \sin\phi e^{\imath k_0(x'\cos\phi+y'\sin\phi)}dx'\right|^2 \tag{5.5}$$

$$\sigma_{TE}(\phi,\phi^i) = \frac{k_0}{4}\left|\int \frac{K_z}{\eta} e^{ik_0(x'\cos\phi+y'\sin\phi)}dx'\right|^2. \tag{5.6}$$

Since double the magnetic source remains at the cavity aperture after applying the method of images, substituting in the electric field further reduces these equations to:

$$\sigma_{TM}(\phi,\phi^i) = \frac{k_0}{4}\left|-2\int E^{TM} \sin\phi e^{\imath k_0(x'\cos\phi+y'\sin\phi)}dx'\right|^2 \tag{5.7}$$

$$\sigma_{TE}(\phi,\phi^i) = \frac{k_0}{4}\left|2\int \frac{E^{TE}}{\eta} e^{ik_0(x'\cos\phi+y'\sin\phi)}dx'\right|^2. \tag{5.8}$$

Computation of far field or RCS quantities is a post-processing step. The computed transmitted fields u_2 and v_2 will be used to compute the strength of the scattered fields at a distance far from the cavity opening. The trick is that to use the standard formula for far field values, it is necessary to have the scattered field at the interface with free space. That is the values of u_0^s and v_0^s at $y = h$ need to be known. The far field formulas become

$$\sigma_{TM}(\phi,\phi^i) = \frac{k_0}{2}\left|\int_{-\infty}^{\infty} u_0^s(x',h)\sin\phi e^{\imath k_0(x'\cos\phi+h\sin\phi)}dx'\right|^2 \tag{5.9}$$

$$\sigma_{TE}(\phi,\phi^i) = \frac{k_0}{2}\left|\int_{-\infty}^{\infty} \frac{i}{\eta\varepsilon\omega}\frac{\partial v_0^s}{\partial y}(x',h) e^{ik_0(x'\cos\phi+h\sin\phi)}dx'\right|^2. \tag{5.10}$$

The computation of these integrals can potentially be difficult since they are over the entire real line. However, evaluation of such an improper integral can be avoided by relating the scattered fields back to the transmitted fields u_2 and v_2.

$$\sigma_{TM}(\phi,\phi^i) = \frac{k_0}{2}\left|\sin\phi e^{\imath k_0(h\sin\phi)}\int_{-\infty}^{\infty} u_0^s(x',h) e^{\imath k_0(x'\cos\phi)}dx'\right|^2 \tag{5.11}$$

$$\sigma_{TE}(\phi,\phi^i) = \frac{k_0}{2}\left|\frac{i}{\eta\varepsilon\omega}e^{\imath k_0(h\sin\phi)}\int_{-\infty}^{\infty} \frac{\partial v_0^s}{\partial y}(x',h) e^{ik_0(x'\cos\phi)}dx'\right|^2 \tag{5.12}$$

Now the integrals are Fourier transforms of u_0^s and $\frac{\partial v_0^s}{\partial y}$. By equation (3.18) the Fourier transform of u_0^s at $y = h$ is $C(\lambda)e^{-\kappa_0 h}$. Solve for $C(\lambda)$ in terms of the known solution u_2 by using equation (3.25) and the continuity at $y = 0$ to arrive at

$$C(\lambda)e^{-\kappa_0 h} = \left[\frac{2\kappa_1 e^{-\kappa_0 h}}{R_{TM}(0)}\right] \mathcal{F}_x[u_2|_{y=0}]. \tag{5.13}$$

Applying the above steps, the far field for TM case takes on these forms:

$$\sigma_{TM}(\phi, \phi^i) = \frac{k_0}{2} \left|\sin\phi e^{\imath k_0 (h\sin\phi)} C(\lambda) e^{-\kappa_0 h}\right|^2 \tag{5.14}$$

$$\sigma_{TM}(\phi, \phi^i) = \frac{k_0}{2} \left|\sin\phi e^{\imath k_0 (h\sin\phi)} \left[\frac{2\kappa_1 e^{-\kappa_0 h}}{R_{TM}(0)}\right] \mathcal{F}_x[u_2|_{y=0}]\right|^2 \tag{5.15}$$

By equation (4.7) the Fourier transform of $\frac{\partial v_0^s}{\partial y}$ at $y = h$ is $-\kappa_0 D(\lambda)e^{-\kappa_0 h}$. $D(\lambda)$ is solved in terms of the known solution for $\frac{\partial v_2}{\partial y}$ at $y = 0$ by using equation (4.10) and the continuity.

$$-\kappa_0 D(\lambda)e^{-\kappa_0 h} = \frac{-2\kappa_1\kappa_0 e^{-\kappa_0 h}}{S_{TE}(0)} \mathcal{F}_x \left[\frac{\varepsilon_1}{\varepsilon_2}\frac{\partial v_2}{\partial y}\bigg|_{y=0}\right] \tag{5.16}$$

Applying the above steps, the far field for TE case takes on these forms:

$$\sigma_{TE}(\phi, \phi^i) = \frac{k_0}{2} \left|\frac{i}{\eta\varepsilon\omega} e^{\imath k_0 (h\sin\phi)} (-\kappa_0) D(\lambda) e^{-\kappa_0 h}\right|^2 \tag{5.17}$$

$$\sigma_{TE}(\phi, \phi^i) = \frac{k_0}{2} \left|\frac{i}{\eta\varepsilon\omega} e^{\imath k_0 (h\sin\phi)} \frac{-2\kappa_1\kappa_0 e^{-\kappa_0 h}}{S_{TE}(0)} \mathcal{F}_x \left[\frac{\varepsilon_1}{\varepsilon_2}\frac{\partial v_2}{\partial y}\bigg|_{y=0}\right]\right|^2. \tag{5.18}$$

Therefore the far field values are completely in terms of the finite element approximations from the cavity using

$$\sigma_{TM}(\phi, \phi^i) = k_0 \left|\sin\phi e^{\imath k_0 (h\sin\phi)} \frac{\kappa_1 e^{-\kappa_0 h}}{R_{TM}(0)} \mathcal{F}_x[u_2|_{y=0}]\right|^2 \tag{5.19}$$

$$\sigma_{TE}(\phi, \phi^i) = k_0 \left|\frac{i}{\eta\varepsilon\omega} e^{\imath k_0 (h\sin\phi)} \frac{\kappa_1\kappa_0 e^{-\kappa_0 h}}{S_{TE}(0)} \mathcal{F}_x \left[\frac{\varepsilon_1}{\varepsilon_2}\frac{\partial v_2}{\partial y}\bigg|_{y=0}\right]\right|^2. \tag{5.20}$$

Also, note that both of the finite element solutions have support limited to $[0, L]$ in the x

direction. Therefore, the integrals performed in the Fourier transforms are performed on a finite interval.

Chapter 6

Numerical Results

This chapter presents figures of the results obtained by applying the FEM. Sections 6.2 displays the RCS signature for various test cases for the TM polarization of a rectangular cavity, while sections 6.3 provides similar results for the TE polarization. The layered methodology suggested by this research was coded using Matlab® and validation testing of the code is provided in sections 6.1 to assure the output can duplicate the signatures of other publications.

Sections 6.2 and 6.3 address the resulting effect of a surface layer on the RCS. To maintain consistency in test parameters for each polarization, the following set of general test cases was implemented:

1. Increasing the dimension of the material layer
2. Increasing the cavity depth
3. Increasing the cavity length.

Each of these test cases is based on either a monostatic or bistatic radar system and will be noted within each description. All monostatic plots were computed using an incident angle ranging between $[0, \frac{\pi}{2}]$. Section 6.4 demonstrates the results produced by some interesting cavity geometries since FEM is capable of handling more complex cavity shapes.

6.1 Validation Testing

When dealing with a rectangular cavity a Fourier based solution can be found. The solution is exact in principle, but in reality it is an approximation due to the truncation of the Fourier series solution. Despite the approximation errors, the Fourier solution is a convenient basis for comparison to verify that the finite element approach is working correctly. The following figures compare the Fourier and finite element solutions at the opening of a rectangular cavity with width 1.25 and depth .2 meters. The angle of incidence is $\pi/3$ radians and the frequency is 3π. The material overlayer is .1 meter thick and consists of material with parameters $\varepsilon_1 = 2$ and $\mu_1 = 2$. The material parameters for the cavity are $\varepsilon_2 = 1 - .5\imath$ and $\mu_2 = 1 - .5\imath$. Both the TM and TE cases provided show a strong agreement.

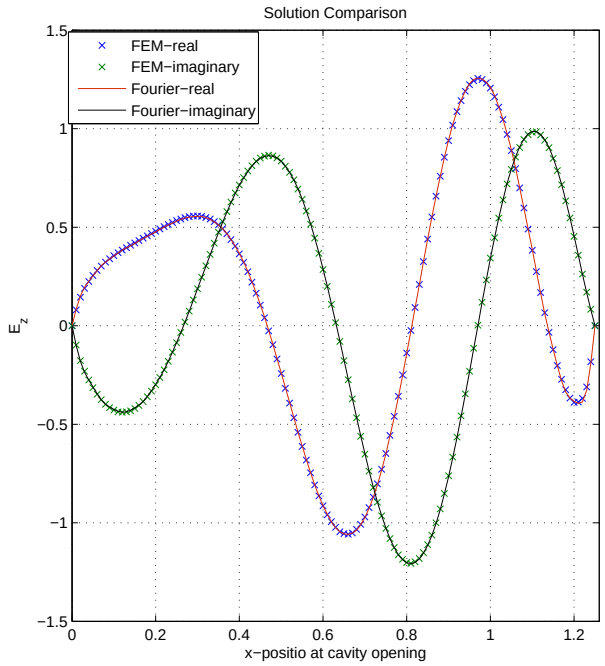

Figure 6.1: Cavity Opening: Fourier vs FEM TM case

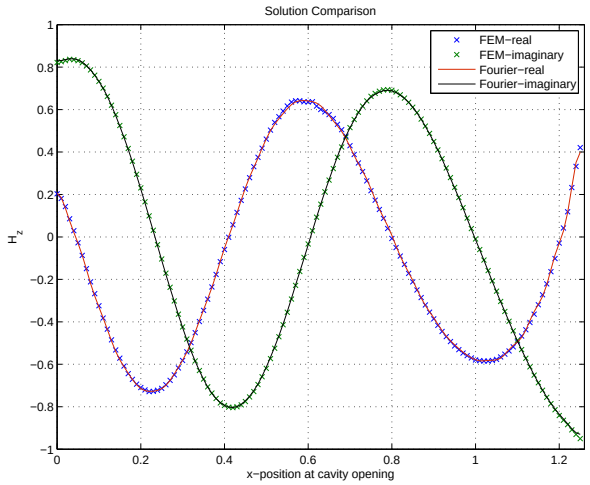

Figure 6.2: Cavity Opening: Fourier vs FEM TE case

The RCS produced from the Fourier and FEM methods are compared in Figures 6.3, 6.4, 6.5 and 6.6. The geometry and parameters are the same as for the comparisons above. As expected, good agreement is demonstrated for both TM and TE polarizations.

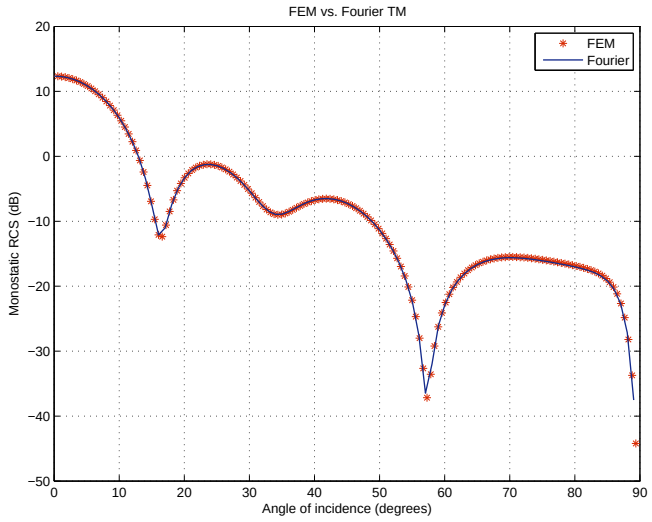

Figure 6.3: Monostatic Cross Section: Fourier vs FEM TM case

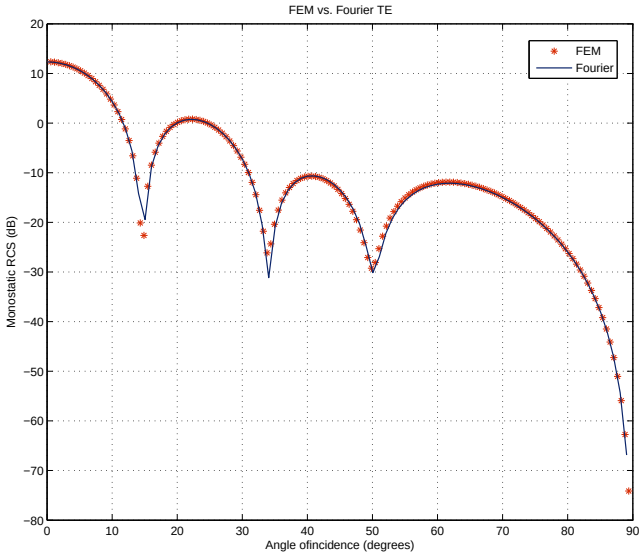

Figure 6.4: Monostatic Cross Section: Fourier vs FEM TE case

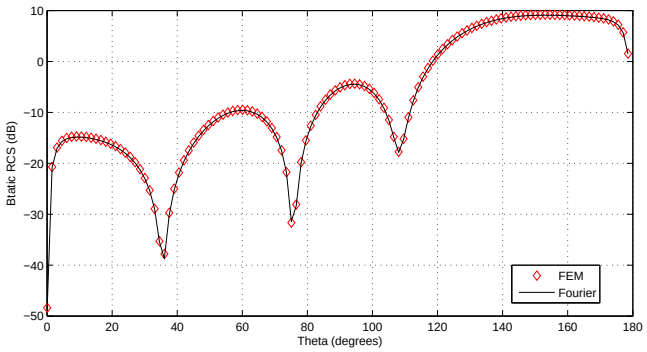

Figure 6.5: Bistatic Cross Section: Fourier vs FEM TM case

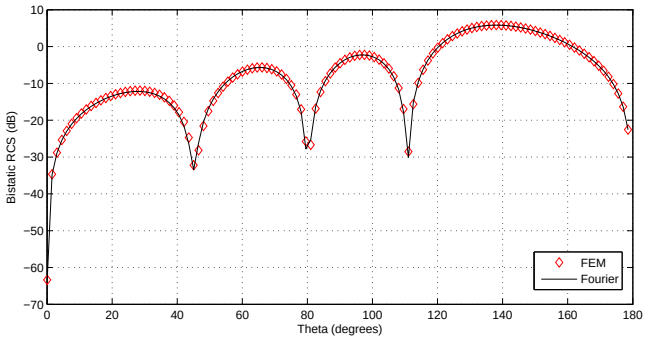

Figure 6.6: Bistatic Cross Section: Fourier vs FEM TE case

6.2 TM: Testing

6.2.1 Increasing the dimensions of the material layer

Monostatic RCS Plots

The tested thickness of the material layer ranges from 0.025 to 1.0 meters with material parameters $\varepsilon_1 = 4$ and $\mu_1 = 1$. This test uses a rectangular cavity of depth 0.5 meters and material parameters $\varepsilon_2 = 1$ and $\mu_2 = 2$. The angle of incidence is $\frac{\pi}{4}$ with frequency 6π. Figure 6.7 shows results of material layer ranging from 0.025 to 0.075 meter while figure 6.8 has a material layer ranging from 0.1 to 1.0.

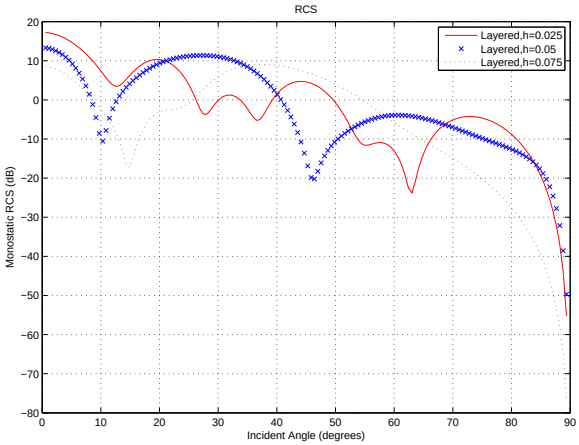

Figure 6.7: Monostatic RCS for TM polarization testing varying thickness parameters of the material surface when $aoi = \pi/4$, $L = 1.25$, $\varepsilon_1 = 4$ and $\mu_1 = 1$

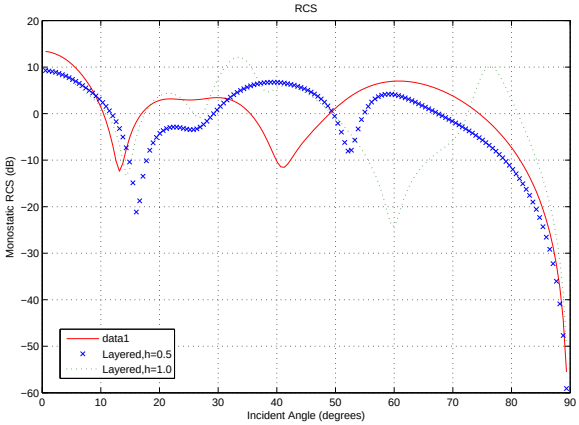

Figure 6.8: Monostatic RCS for TM polarization testing varying thickness parameters of the material surface when $aoi = \pi/4$, $L = 1.25$, $\varepsilon_1 = 4$ and $\mu_1 = 1$

6.2.2 Increasing the cavity depth

Monostatic RCS Plots

The tested depth of a rectangular cavity ranges from 0.2 to 5.5 meters with material parameters $\varepsilon_2 = 2$ and $\mu_2 = 1$. This test uses 0.1 meters thick material layer with parameters $\varepsilon_1 = 4$ and $\mu_1 = 1$. The angle of incidence is $\frac{\pi}{4}$ with frequency 6π. Figure 6.9 shows results of cavity depth 0.2, 1.2 and 3.2 meters while figure 6.10 illustrates cavity depth of 0.5, 3.0 and 5.5.

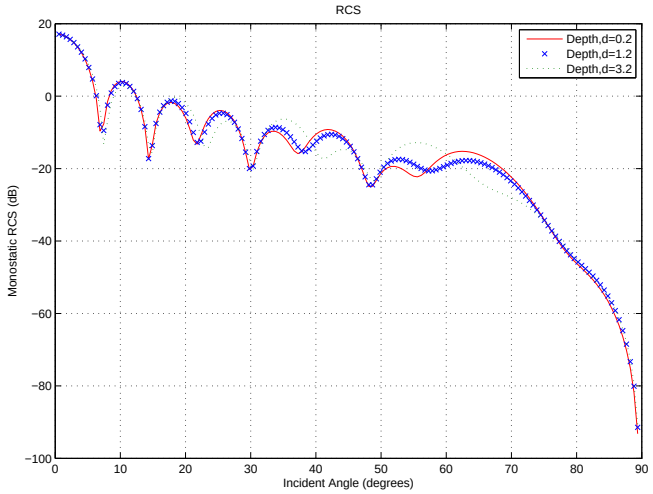

Figure 6.9: Monostatic RCS for TM polarization testing varying depth parameters of the material surface when $aoi = \pi/4$, $L = 1.25$, $\varepsilon_1 = 4$ and $\mu_1 = 1$

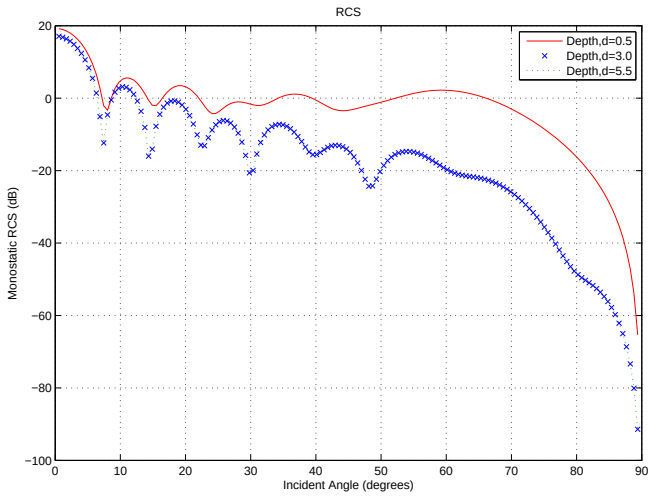

Figure 6.10: Monostatic RCS for TM polarization testing varying depth parameters of the material surface when $aoi = \pi/4$, $L = 1.25$, $\varepsilon_1 = 4$ and $\mu_1 = 1$

6.2.3 Increasing the cavity length

Monostatic RCS Plots

The tested length of the opening of a rectangular cavity ranges from 0.25 to 5.25 meters. The cavity filled with a material of parameters $\varepsilon_2 = 1$ and $\mu_2 = 2$ is covered with a 0.1 meter thick material layer with parameters $\varepsilon_1 = 16 - 5\imath$ and $\mu_1 = 4 - 1.25\imath$. The angle of incidence is $\frac{\pi}{3}$ with frequency 4π. Figure 6.11 shows results of all cavity opening ranges.

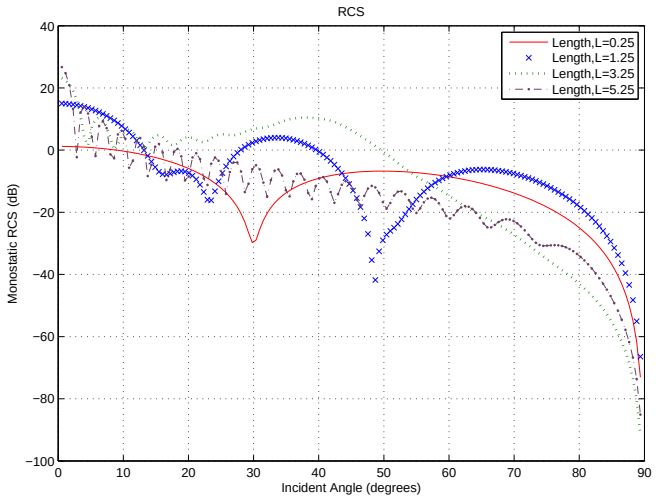

Figure 6.11: Monostatic RCS for TM polarization testing varying length of the cavity opening to the upper half plane with layer parameters of $\varepsilon_1 = 16 - 5\imath$ and $\mu_1 = 4 - 1.25\imath$ with $aoi = \pi/3$.

6.3 TE: Testing

6.3.1 Increasing the dimensions of the material layer

Monostatic RCS Plots

TE polarization was tested with the same parameters as TM polarization. The tested thickness of the material layer ranges from 0.025 to 1.0 meter with material parameters $\varepsilon_1 = 4$ and $\mu_1 = 1$. This test uses a rectangular cavity of depth 0.5 meters and material parameters $\varepsilon_2 = 1$ and $\mu_2 = 2$. The angle of incidence is $\frac{\pi}{4}$ with frequency 6π. Figure 6.12 shows results of material layer from 0.025 to 0.075 meter while figure 6.13 material layer ranges from 0.1 to 1.0.

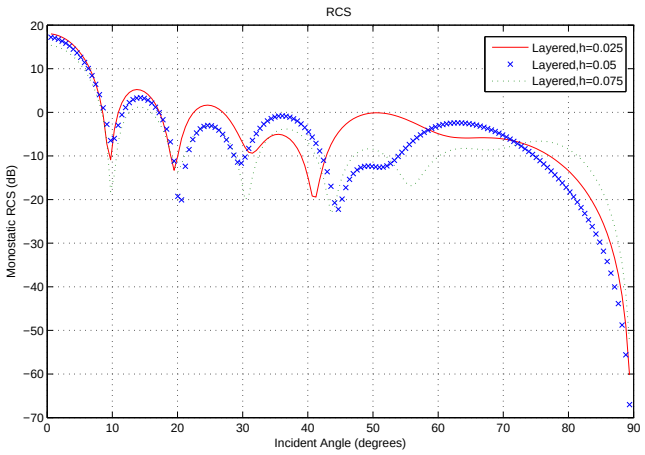

Figure 6.12: Monostatic RCS for TE polarization testing varying thickness parameters of the material surface when $aoi = \pi/4$, $L = 1.25$, $\varepsilon_1 = 4$ and $\mu_1 = 1$

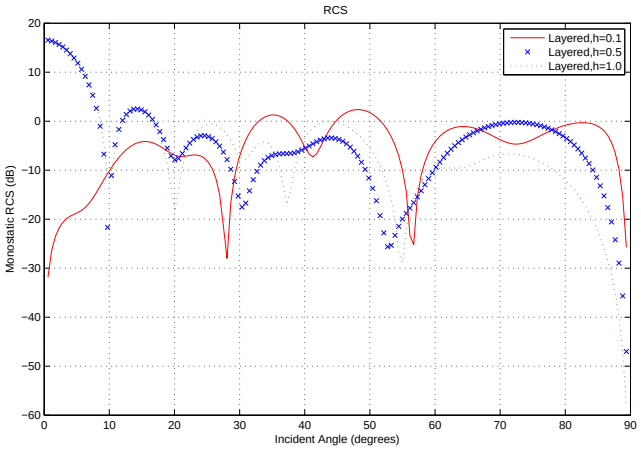

Figure 6.13: Monostatic RCS for TE polarization testing varying thickness parameters of the material surface when $aoi = \pi/4$, $L = 1.25$, $\varepsilon_1 = 4$ and $\mu_1 = 1$

6.3.2 Increasing the cavity depth

Monostatic RCS Plots

As in the TM polarization, the tested depth of a rectangular cavity ranges from 0.2 to 5.5 meters with material parameters $\varepsilon_2 = 2$ and $\mu_2 = 1$. This test uses 0.1 meter thick material layer with parameters $\varepsilon_1 = 4$ and $\mu_1 = 1$. The angle of incidence is $\frac{\pi}{4}$ with frequency 6π. Figure 6.14 shows results of cavity depth 0.2, 1.2 and 3.2 meters while figure 6.15 illustrates cavity depth of 0.5, 3.0 and 5.5 meters.

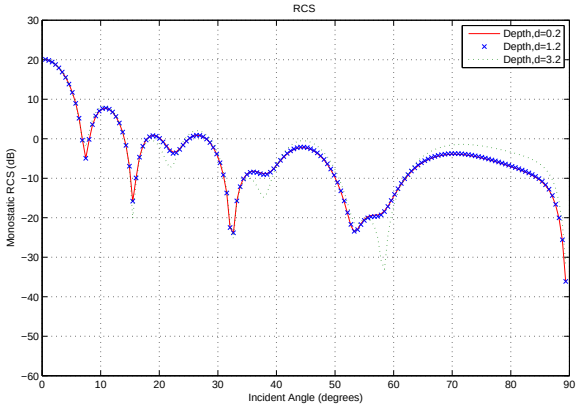

Figure 6.14: Monostatic RCS for TE polarization testing varying depth parameters of the material surface when $aoi = \pi/4$, $L = 1.25$, $\varepsilon_1 = 4$ and $\mu_1 = 1$

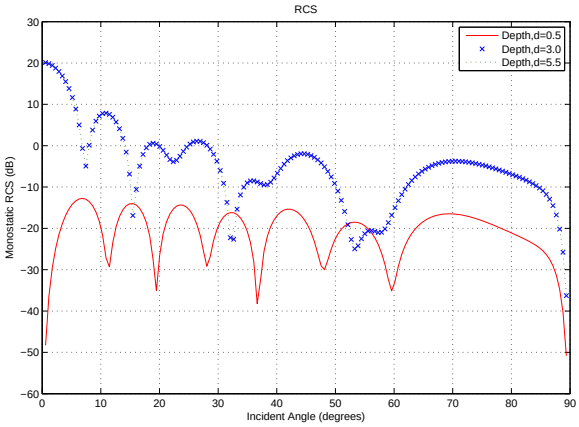

Figure 6.15: Monostatic RCS for TE polarization testing varying depth parameters of the material surface when $aoi = \pi/4$, $L = 1.25$, $\varepsilon_1 = 4$ and $\mu_1 = 1$

6.3.3 Increasing the cavity length

Monostatic RCS Plots

The tested length of the opening of a rectangular cavity ranges from 0.25 to 5.25 meters. The cavity is filled with a material having these parameters: $\varepsilon_2 = 1$ and $\mu_2 = 2$. This test uses 0.1 meter thick material layer with parameters $\varepsilon_1 = 16 - 5\imath$ and $\mu_1 = 4 - 1.25\imath$. The angle of incidence is $\frac{\pi}{3}$ with frequency 4π. Figure 6.16 shows results of all cavity opening ranges.

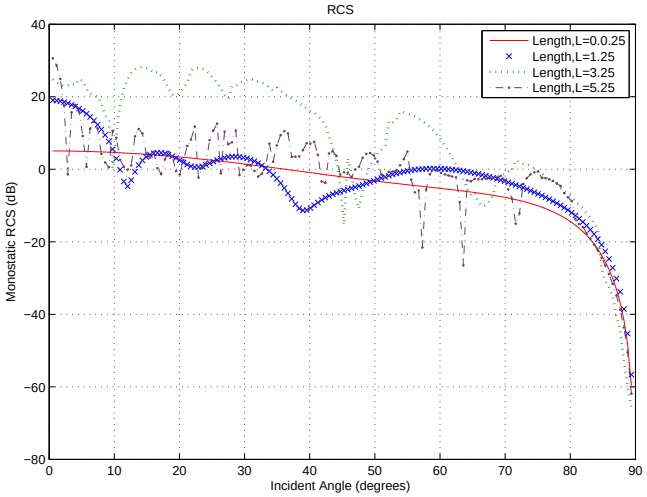

Figure 6.16: Monostatic RCS for TE polarization testing varying length of the cavity opening to the upper half plane with layer parameters of $\varepsilon_1 = 16 - 5\imath$ and $\mu_1 = 4 - 1.25\imath$ with $aoi = \pi/3$.

6.4 Numerical Experiments

The comparison with the Fourier results shows that the finite element formulation gives correct results for the rectangular cavity underneath a material layer. The remaining figures will demonstrate the results produced by some interesting cavity geometries with a variety of parameters. All cases use the opening length of 1 unit and the frequency of the incident field is 8π.

6.4.1 Triangle

The first experiment is a triangular filled cavity with material parameters $\varepsilon_2 = 1$ and $\mu_2 = 2$. The material overlayer has thickness .3 meter and the material parameters $\varepsilon_1 = 1 + 0.1\imath$ and $\mu_1 = 2$. The angle of incident field is $\pi/3$. The first two figures are the results for the TM case. The absolute value of the field in the cavity is shown in the first figure and the monostatic radar cross section for the field is given in the second figure.

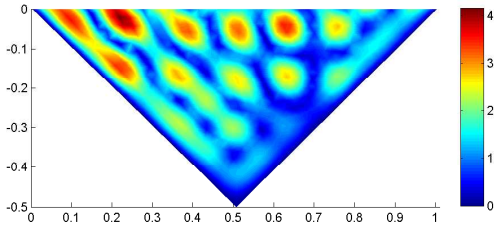

Figure 6.17: Absolute Value: TM Triangular Geometry

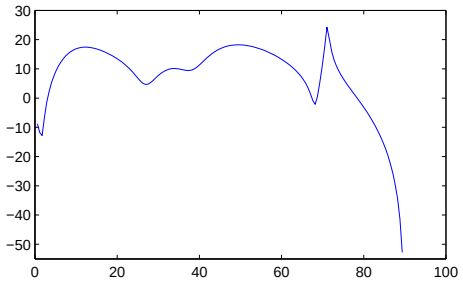

Figure 6.18: Monostatic Cross Section: TM Triangular Geometry

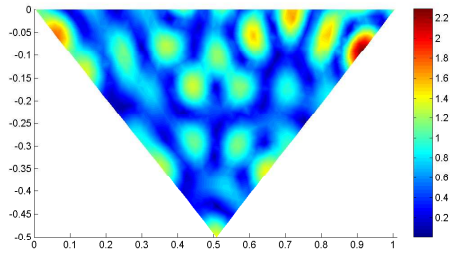

Figure 6.19: Absolute Value: TE Triangular Geometry

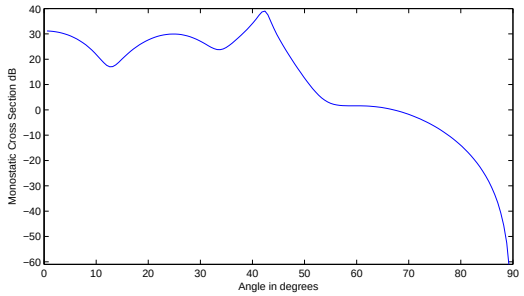

Figure 6.20: Monostatic Cross Section: TE Semicircular Geometry

6.4.2 Semicircle

The second experiment is a semicircular filled cavity with material parameters $\varepsilon_2 = 1$ and $\mu_2 = 2$. The material overlayer has thickness .1 meter and material parameters $\varepsilon_1 = 16 + 5\imath$ and $\mu_1 = 4 - 1.25\imath$. The angle of the incidence field is $\pi/4$. The first two figures are the results of the TM case. The absolute value of the field in the cavity is shown in the first figure and second figure represents the monostatic radar cross section for the field.

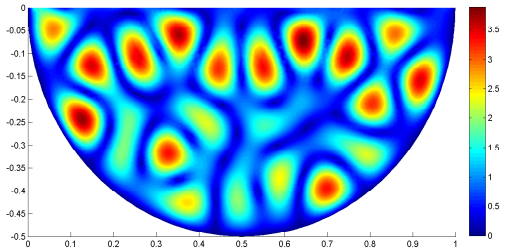

Figure 6.21: Absolute Value: TM Semicircular Geometry

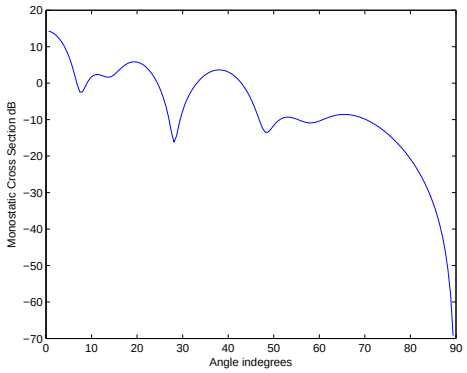

Figure 6.22: Monostatic Cross Section: TE Semicircular Geometry

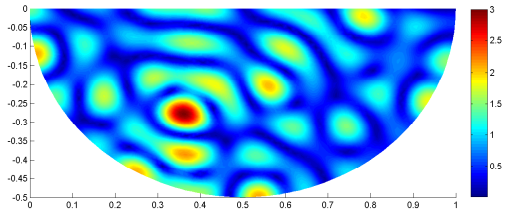

Figure 6.23: Absolute Value: TE Semicircular Geometry

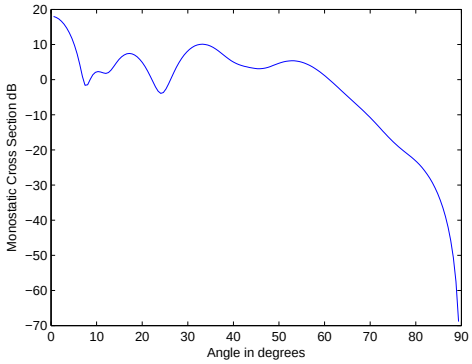

Figure 6.24: Monostatic Cross Section: TE Semicircular Geometry

6.4.3 Random Polygon

In order to get away from the classic geometric shapes, the third experiment is an arbitrarily polygonal figure with material parameters $\varepsilon_2 = 2$ and $\mu_2 = 1$. The material overlayer has thickness .2 meter and the material parameters $\varepsilon_1 = 3$ and $\mu_1 = 2$. The angle of incident field is 0 radians. The first two figures are the results for TM case. The absolute value of the field in the cavity is shown in the first figure and the second figure represents the monostatic radar cross section for the field.

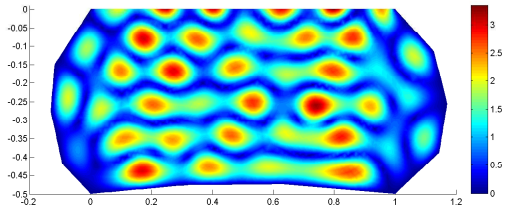

Figure 6.25: Absolute Value: TM Third Cavity

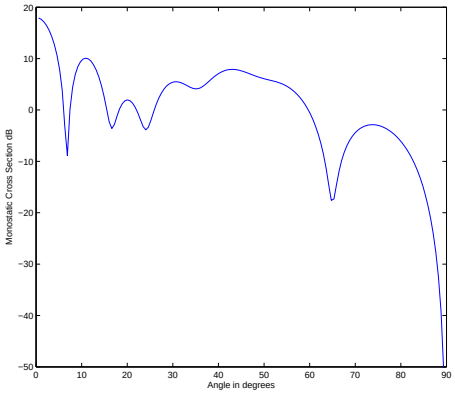

Figure 6.26: Monostatic Cross Section: TM Third cavity

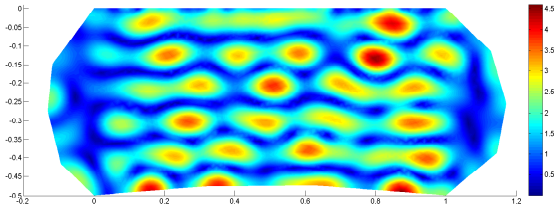

Figure 6.27: Absolute Value: TE Third Cavity

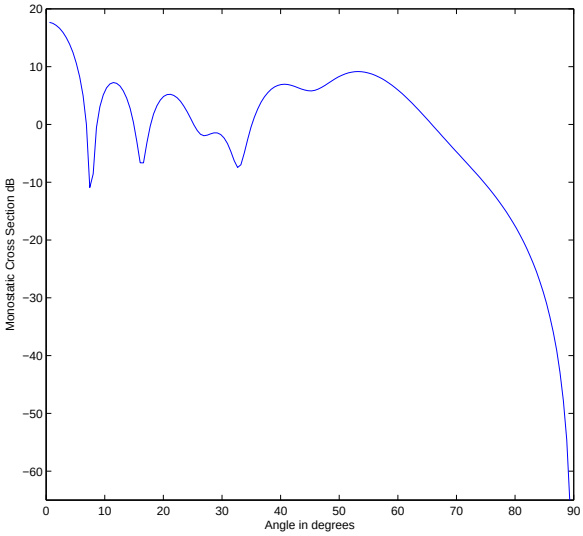

Figure 6.28: Monostatic Cross Section: TE Third cavity

Chapter 7

Conclusion and Future Work

The problem of an electromagnetic cavity beneath a uniform dielectric layer can now be modeled with the FEM. The representation of the incoming fields, the scattered and transmitted fields, along with a transparent boundary condition which can be incorporated into the FEM, are provided here. In addition, it has been shown how to compute the far field values in terms of the computed finite element solution. Methods solving for the TM and TE polarizations were both explored. The results offer the ability of predicting RCS for complex geometries.

In the examples displayed in Chapter Six, the parameters defining the material coating above the half plane and inside the rectangular cavity present two types of materials, a conductive ($\varepsilon_r = 16 - 5\imath$, $\mu_r = 4 - 1.25\imath$) and non-conductive layer ($\varepsilon_r = 4$, $\mu_r = 1$). The results of coating the surface with a conductive material are similar for the TE and TM polarizations, with a trend showing that as the material layer thickens, the strength of the return echo weakens. This is consistent in the monostatic and bistatic signatures. Coating the surface with a non-conductive material results in an inconsistent behavior, but usually reveals an increase in the strength of the return signal.

When time is a consideration, this methodology offers a reasonable approximation but the computation is very time consuming.

There exist a number of avenues that are yet to be explored given this base model. In the future, the problem should be considered in the time domain. Also, the problem should

be studied for three-dimensional cavities in both the frequency and time domain. One last advancement is testing the effect of multiple material layers above the half plane on the output of the RCS in both domains.

Bibliography

[1] H. Ammari, G. Bao, and A. Wood. An integral equation method for the electromagnetic scattering from cavities. *Mathematical Methods for Applied Science*, 23:1057–1072, 2000.

[2] H. Ammari, G. Bao, and A. Wood. Analysis of the electroagnetic scattering from a cavity. *Japan Journal of Industrial and Applied Mathematics*, 23(2):301–308, 2001.

[3] H. Ammari, G. Bao, and A. Wood. A cavity problem for maxwell's equations. *Methods and Applications of Analysis*, 9(2):249–260, 2002.

[4] Kasra Barkeshli and John L. Volakis. Scattering by an aperature formed by a rectangular cavity in a ground plane. Technical report, University of Michigan Radiation Laboratory Report 389757-2-T, December 1989.

[5] James L. Blackshire, Charles Buynak, Gary Steffes, and Rob Marshall. Nondestructive evaluation through aircraft coatings: a state-of-the-art assessment. In *Joint FAA/DoD/NASA Aging Aircraft Conference*, Atlanta, Georgia, March 2006.

[6] R. J. Burholder. Two ray shooting methods for computing em scattering by a large open ended cavities. *Computer Physics Communications*, 68:353–365, 1991.

[7] J. L. Fleming and J. Moser. A fourier approach to model electromagnetic fields scattered by a burried cavity. *Submitted for Publication*, January 2009.

[8] J. L. Fleming and N. Pernischova. A finite element approach to model electromagnetic fields scattered by a buried cavity. *Submitted for Publication*, 2009.

[9] G. W. Hanson and A. B. Yakovlev. *Operator Theory for Electromagnetics: An Introduction*. Springer, New York, 2001.

[10] Daniel J. Hoppe and Yahya Rahmat-Samii. *Impedance Boundary Conditions In Electromagnetics*. Taylor & Francis, Washington DC, 1995.

[11] S. A. Hovanessian and L.A. Pipes. *Digital Computer Methods in Engineering*. McGraw-Hill, New York, 1969.

[12] Eric Howe. Analysis and numerical solution of an integral equation method for electromagnetic scattering from a cavity in a ground plane. Master's thesis, Air Force Institute of Technology, April 2001.

[13] J. Jin. *The Finite Element Method in Electromagnetics*. Wiley, New York, 1993.

[14] J.M. Jin. Electromagnetic scattering from large deep and arbitrarily shaped open cavity. *Electromagnetics*, 18(1):3–34, 1998.

[15] J.M. Jin, S. Ni, and S.W. Lee. Hybridization of srb and fem for scattering by large bodies with cracks and cavities. *IEEE Transactions on Antennas and Propagation*, 43(10):1130–1139, 1995.

[16] J.M. Jin and J.L. Volakis. A hybrid finite element method for scattering and radiation by microstrip path antennas and arrays residing in a cavity. *IEEE Transactions on Antennas and Propagation*, 39(11):1598–1604, 1991.

[17] L.C. Kempel and T.B.A. Senior. Scattering by a small cavity-backed hole. *IEEE Transactions on Antennas and Propagation*, 41(8):1115–1121, 1993.

[18] L.C. Kempel and J.L. Volakis. Scattering by cavity backed antennas on a circular cylinder. *IEEE Transactions on Antennas and Propagation*, 42(9):1268–1279, 1994.

[19] J. Liu and J.M. Jin. A special higher order finite element method for scattering by deep cavities. *IEEE Transactions on Antennas and Propagation*, 48(5):694–703, 2000.

[20] M. A. Morgan. Mode expansion solution for scattering by a material filled rectangular groove. *Progress In Electromagnetic Research*, 98(PIER 18):1–17, 1998.

[21] Jessica L. Moser. A fourier solution for electromagnetic scattering by a covered rectangular cavity. Master's thesis, Duquesne University, Pittsburgh, Pennsylvania, July 2008.

[22] Tah J. Park, Hyo J. Eom, and Kuniaki Yoshitomi. An analytic solution for transverse-magnetic scattering from a rectangular channel in a conducting plane. *Journal of Applied Physics*, 73(7):3571–3573, 1992.

[23] Tah J. Park, Hyo J. Eom, and Kuniaki Yoshitomi. An analysis of TE-scattering from a rectangular channel in a conducting plane. *Radio Science*, 28(5):663–673, 1993.

[24] Andrew F. Peterson, Scott L. Ray, and Raj Mittra. *Computational Methods for Electromagnetics*. Institute of Electrical and Electronics Engineers, Inc., New York, 1998.

[25] Mathew N.O. Sadiku. *Numerical Techniques in Electromagnetics*. CRC Press LLC, Boca Raton, Florida, 2001.

[26] Merrill Skolnik. An introduction to radar. In *Radar Handbook*, pages 1.1–1.21. McGraw Hill, Cambridge, 1990.

[27] Glenn Smith. *An Introduction to Classical Electromagnetic Radiation*. Cambridge University Press, Cambridge, 1997.

[28] Tri Van and Aihua Wood. Finite element analysis of electromagnetic scattering from a cavity. *IEEE Transactions on Antennas and Propagation*, 51(1):130–137, January 2003.

[29] A. Wood. Numerical simulation of electromagnetic scattering induced by an overfilled cavity in the ground plane. *IEEE Transactions on Antennas and Wireless Propagation Lttrs.*, 4:224–228, 2005.

[30] Aihua Wood. Analysis of electromagnetic scattering from an overfilled cavity in the ground plane. *Journal of Computational Physics*, 215:630–641, 2006.

[31] W.D. Wood and A.W. Wood. Developent and numerical solution of integral equations for electromagnetic scattering from a rough trough in a ground plane. *IEEE Transactions on Antennas and Propagation*, 47(8):1318–1322, 1999.

[32] William Wood. *Electromagnetic Scattering from a Cavity in a Ground Plane: Theory and Experiment*. PhD thesis, Air Force Institute of Technology, March 1999.